

1 **TITLE:**

2 Atomic Force Microscopy on a multiplexed SPRi chip: a rigorous methodology for a deep
3 qualification of extracellular vesicles subsets

4

5 **AUTHORS AND AFFILIATIONS:**

6 Geetika Raizada¹, Balasubramaniam Namasivayam², Sameh Obeid³, Wilfrid Boireau¹, Eric
7 Lesniewska⁴, Celine Elie-Caille^{1*}

8

9 ¹FEMTO-ST Institute, CNRS UMR-6174, Université de Bourgogne Franche-Comté, 15B Av. des
10 Montboucons, 25030 Besançon, France

11 ²Lille Neuroscience & Cognition research centre (Inserm U1172), Lille, France

12 ³Paris sud University, Chatenay- Malabry, France

13 ⁴Interdisciplinary Lab Carnot Bourgogne LICB, CNRS UMR-6303, Université de Bourgogne
14 Franche-Comté 9 Av. Alain Savary, 21078 Dijon, France

15

16 **SUMMARY:**

17 We propose a new generation of multiparametric analytical platform with increased throughput
18 for the characterization of extracellular vesicles (EVs) subsets. Our method is based on a
19 combination of multiplexed biosensing method with metrological, morphomechanical analysis
20 by AFM, coupled with Raman spectrometer, to qualify vesicular targets trapped on a microarray
21 biochip.

22

23 **ABSTRACT:**

24 Extracellular vesicles (EVs) are membrane-derived tiny vesicles, produced by all cells, that range
25 from 50 to several hundred of nanometers in diameter, and used as means of intercellular
26 communication. They are emerging as promising diagnostic and therapeutic tools for a variety of
27 diseases. There are two main biogenesis processes used by cells to produce EV, giving EVs
28 presenting differences in size, composition and content. Due to their high complexity - in size,
29 composition and cell origin -, their characterization requires a combination of analytical
30 techniques. Our project consists in developing a new generation of multiparametric analytical
31 platform with increased throughput for the characterization of subpopulations of extracellular
32 vesicles (EVs). To reach this goal, we start from the nanobioanalytical platform (NBA) established
33 in the group, which allows an original investigation of EVs based on a combination of multiplexed
34 biosensing method with metrological and morphomechanical analysis by AFM of vesicular targets
35 trapped on a microarray biochip. We aim to complete this EVs investigation with a phenotypic
36 and molecular analysis by Tip Enhanced Raman spectroscopy (TERS). The objective is to propose
37 a multimodal and easy to use analytical solution to reach a deep qualification of EVs subsets in
38 biological fluids with clinical prospects.

39

40 **INTRODUCTION:**

41 The infatuation in EVs research, combined with the challenges this field faces, has resulted in the
42 development and implementation of a large variety of approaches and techniques for quantifying
43 or characterizing these vesicles. None of these techniques, on their own, however, gives all the
44 information allowing to characterize EVs subsets. The inherent heterogeneity of EVs, the diversity

45 of their biochemical & physical properties, prevents to get global analyses that are reliable and
46 reproducible, especially for EVs contained in a mixture (crude sample). Detection and
47 characterization methods EVs are therefore needed, individually and generally used
48 systematically, in complement of the other methods, faster, but not selective [1].

49
50 High-resolution imaging, by transmission electron microscopy (TEM and cryoTEM) or atomic
51 force microscopy (AFM), allows to determine the morphology and metrology of EVs with a
52 nanometric resolution [2-7]. However, the main limitation of the use of electron microscopy for
53 biological objects, such as EVs, reside in the need for a vacuum to carry out the exploration, which
54 requires fixation and dehydrating the sample. Such preparation makes it difficult to transpose
55 from the structures observed to the in solution EVs morphology. In order to avoid this
56 dehydration of the sample, the technique of cryoTEM is the most widely used for EV
57 characterization [8]. It is widely used for determine the ultrastructure of EVs. Immunolabelling of
58 vesicles by biofunctionalized gold nanoparticles also make it possible to identify specific sub-
59 populations of EVs and discriminate against them from others particles present in a complex
60 biological sample. However, the low number of EVs analyzed by electronic microscopy, often
61 makes difficult a characterization that is representative of a complex and heterogeneous sample.

62
63 To reveal this size heterogeneity, minimal information initiative for studies of extracellular
64 vesicles of ISEV international community suggests analyzing a sufficient number of images of
65 wide field, accompanied by more surface images reduced, revealing with high resolution EVs
66 Individual [9].

67
68 Atomic force microscopy (AFM) occurs as an alternative to optical approaches and electronic
69 diffraction techniques for the study of EVs. This technique uses a sharp tip hold by a flexible
70 cantilever that scans the sample deposited on one support, line by line, adjusting the distance
71 between the tip and the elements present, thanks to a feedback loop. It makes it possible to
72 characterize the topography of the sample and to collect morphomechanical information [10-
73 13]. The EVs can be scanned by AFM, either after being deposited on an atomically flat substrate,
74 or after have been captured on a specific substrate functionalized by antibodies, peptides or
75 aptamers, to characterize the various subpopulations [13-14]. By its ability to quantify and to
76 simultaneously probe the structure, the biomechanics and the biomolecular content of EVs
77 within complex biological samples, without the need for pre-treatment, labelling, or
78 dehydration, the AFM is now increasingly used to characterize EVs in a fine and multiparametric
79 way, under physiological conditions of temperature and medium.

80
81 We propose here a methodology using a central gold biochip, with its capability to be
82 (bio)chemically functionalized in a multiplexed format. This substrate consists in the corner stone
83 of a powerful analytical platform combining biodetection of EVs subsets by surface plasmon
84 resonance and atomic force microscopy metrology and morphomechanical characterization. This
85 paper will show readers that combination of powerful technics assisted by a highly rigorous
86 methodology in substrate preparation and data acquisition, makes the EVs analysis deep, resolve
87 and robust.

88

89 **PROTOCOL:**

90

91 The principle of our approach is to prepare a gold substrate, to adsorb/graft or capture EVs
92 subtypes, for their characterization in terms of phenotypes, size and morphology. This substrate
93 can indeed present 3 types of interfaces, of growing complexity : naked, chemically functionalized
94 or ligand microarrays.

95

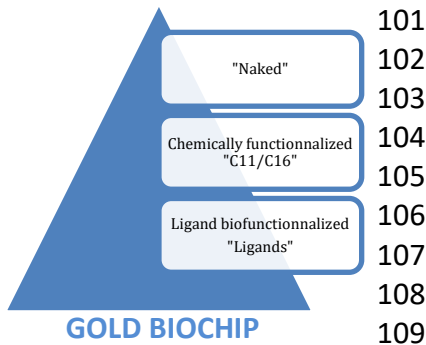
96 Before describing the different steps of the protocol, here is presented schematically in figure 1
97 our NBA approach, coupling SPRI, AFM and Spectroscopy.

98

99

[Here Figure 1]

100



110

111

112 All the details/procedure is given below, but we propose here to present for which reasons and
113 applications 3 types of biochip are generated:

114

115 **Naked biochip:** it enables the simple adsorption of EVs on gold : it is possible to play with the
116 buffer used and to realize this adsorption either in a passive way (incubation then rinsing steps),
117 or under flow (in SPRI). Moreover, this adsorption in passive way can be realized either on the
118 whole chip (as a macroarray), or localized in microarrays thanks to a micropipette spotter. The
119 “under flow procedure”, allows to follow the kinetics and the level of EVs adsorption. This
120 approach on naked gold substrate is engaged when the chemical layer interface may interfere
121 with the analytical method (i.e. for Raman spectroscopy in our case).

122

123 **Chemically fonctionnalized biochip:** the chemically functionalized biochip is used to create a
124 dense “carpet” of EVs covalently bound on the gold surface, when the objective is to have a global
125 view of the EVs sample. Indeed, in this case, the gold is functionalized by a thiolate mixture, and
126 part of the thiolates are chemically activated to establish covalent binding with targets. Again,
127 this strategy can be realized either in a passive way (incubation then rinsing steps / either in
128 “macroarray” or in multiple microarrays thanks to a micropipette spotter), or under flow (in SPRI)
129 to follow the kinetics and level of EVs grafting on the gold surface.

130

131 **Ligand biofonctionnalized biochip:** the chemically functionalized biochip is here also chemically
132 activated but to covalently graft different ligands (antibodies, receptors, ...), in order to capture

133 by affinity and selectively different EVs subsets coexisting in the biological sample.

134

135 **1. Gold substrate preparation**

136

137 The three types of surface are produced on Gold chip: 1) naked surface, 2) chemically
138 functionalized C11/C16, and 3) biofunctionalized (ligands grafted on C11C16 layer). We will call
139 them “naked”, “C11C16”, and “ligands” respectively from now onwards.

140

141 **Gold Substrate preparation:** The gold biochips were manufactured in-house in the clean room
142 (at the “MIMENTO” Technology Center, Besançon, France). The home-made biochips are
143 composed of glass slides (SF11) with the coating of chromium (2nm Cr) and gold (48nm Au). The
144 coating was done by Physical Vapor Deposition (PVD) with the help of Plassys DC magnetron
145 sputtering. The length of the biochip was 28 mm, width 12.5 mm, and thickness 0.5mm [15].

146

147 **Chemical functionalization:** the naked chips were functionalized by incubating overnight in the
148 mixture of mercapto-1-undecanol (11-MUOH : “C11”) & mercapto-1-hexadecanoic acid (16-MHA
149 “C16”) 90%/10% by mole respectively reaching 1 mM in absolute ethanol, under agitation at
150 room temperature. This step will form a stable Self Assembled Monolayer (SAM), which is useful
151 in grafting of ligands. The biochips were cleaned with absolute ethanol and ultrapure water, then
152 subsequently dried and stored under clean-room conditions.

153 **Activation and EVs or ligand grafting on chemically functionalized biochip :** the biochip was
154 cleaned with ultra-pure water and then to activate C16 carboxylic groups, it was incubated in the
155 mixture of 200 mmol/L EDC and 50 mmol/L Sulfo-NHS for at least 30minutes before the
156 experiments.

157 To immobilize EVs or ligands on the chip, after EDC-NHS activation, we then go either, in passive
158 way to get a macroarray (through one single drop) or a microarrays format (thanks to a
159 micropipette spotter), or under flow, to graft on the whole surface the EVs or ligands. This
160 constitutes our EVs or “ligands” modified chips.

161

162 **[Here Figure 2]**

163

164 For ligand grafting, the molecules were diluted at 200µg/ml, in their optimal pH solution. The
165 optimum pH for grafting antibodies was determined previously by pre-concentration
166 experiments done on SPR-Biacore 3000 instrument from GE Healthcare/now Cytiva life sciences.
167 It should also be noted that the grafting conditions will change with clones of antibodies that we
168 are using, it is therefore recommended to determine the conditions before moving to SPRi
169 experiments.

170 After activation of the chip, 300 nl of EVs/ligand solution was added by using spotter as shown in
171 the figure 2.

172

173 Note: A piece of paper submerged in water should be kept in the both left and right wells to avoid
174 the evaporation of droplets. This step is important to maintain the EVs/ligands in the optimum
175 condition for their stability and functionality.

176

177 After spotting, the biochip was kept under a sonic bath (frequency 37 kHz, and power 30%) for
178 30 min incubation.

179 The biochip was washed from top with ultra-pure water and then was placed on a prism, which
180 is of the same refractivity index (RI) as the biochip.

181 While adjusting the biochip on the top of the prism, a droplet (~ 2.3 μ l) of oil was used which has
182 the same RI as that of the prism to create an uniform thin layer between the biochip and the
183 prism. This step was done to have a continuous medium of the same RI in the optical path.

184 Note: It is important to avoid incorporating any bubble in the oil layer at this step, as it will change
185 the optical properties in the path and will hinder further analysis.

186 **2. Surface Plasmon Resonance imaging**

187

188 SPRi Plex II from Horiba Scientific was used for this experiment. The biochip was mounted on the
189 SPRi-plex system. The flow rate of the buffer was kept at 50 μ l/min.

190 Note: In case of any bubbles, increase the flow rate up to 500-1000 μ l/min; also inject Octyl
191 Glucoside (OG) 40 mM frequently to remove them as soon as possible.

192 **Conditioning of the gold biochip:** Afterwards CCD image acquisition was performed to define the
193 Region of Interest (ROI) as well as the ligand families (when multiplexed biochips is used).

194 The plasmon curves were obtained. In the case of a passivating step (thanks to albumin)
195 performed inside the apparatus, we recommend selecting a working angle to get the optimum
196 sensitivity towards the surface, thus establishing a quality control of the surface reactivity.

197 Note: this passivation step is important when the chip is prepared for affinity/capture
198 biodetection, in order to reduce non-specific interaction between the sample and biochip
199 surface.

200 The kinetic monitoring was chosen. The RSA (200 μ g/ml, prepared in Acetate buffer pH 4.5) was
201 injected at 50 μ l/min for 4 min, which was followed by the injection of Ethanolamine (1M) at 20
202 μ l/min for 10 min, to deactivate the carboxylic groups still present and reactive on the surface.
203 The biochip was then washed by injecting OG 40mM at 50 μ l/min for 4min.

204

205 **Sample Injection:** the Plasmon curves were redefined after passivation and the working angle
206 was chosen according to the ligand this time. In kinetic monitoring, we reduced the flow rate to

207 20 µl/min and waited for the baseline to be stable. The sample was injected at a concentration
208 of choice generally for 10 min, the kinetics of interaction is followed and the reflectivity variation
209 was measured at the end of injection.

210 The different samples that were injected will be described in the results section.

211

212 **After sample injection** : there are 2 ways to finish the SPRi experiment :

213 1st way “unfixed/in liquid”: we take out the biochip from the SPRi apparatus, maintaining a liquid
214 drop on it and go for further AFM characterization of the surface in liquid

215 2nd way “fixed”: glutaraldehyde (0.5%) diluted in water was injected at 20 µl/min for 10 min to
216 fix the objects captured on the biochip. Then water is injected to rinse the surface and the biochip
217 is taken out and washed very gently with distilled water and then air dried to be further analyzed
218 under AFM.

219

220 **3. Atomic Force Microscopy (AFM)**

221

222 Bruker-JPK NanoWizard® 3 Bioscience AFM was used for AFM characterization. Contact mode
223 was used to scan the biochip, in air. Quantitative Imaging mode is used to scan the biochip in
224 liquid conditions. To identify the position of the respective microspots on the biochip, a glass
225 slide with a mask was used. The biochip was then aligned on the top of this mask as shown in the
226 below picture.

227

228

[Here Figure 3]

229

230 **Positioning of the tip:** Using the CCD camera on top of the AFM was used to localize the
231 cantilever on the correct spot that we want to scan. We used triangular shaped cantilever with
232 200 µm length, 28 µm width, and a spring constant of 0.08 N/m. The laser was then aligned on
233 the top of the cantilever, at a position to have an optimum response in the feedback control
234 mechanism.

235

236 **Scanning:** Once engaged and in contact on the biochip surface, the AFM acquisition started, in
237 contact or in quantitative imaging mode, from 3 to 5 big area (typically 10 x 10 µm²) to small area
238 (1 x 1 µm²). The aim is a) to get an AFM characterization that is representative of the whole mm²
239 spot, and 2) to visualize enough EVs and at a good resolution to have a robust analysis (a
240 minimum of 300 EVs counted and analyzed for each condition), to make metrology and
241 morphology measurements.

242 These AFM images were then further processed with JPK Data processing software, and treated
243 thanks to Gwyddion or Mountains SPIP ones.

244 **AFM image treatment:**

245 The AFM images were treated with JPK Data processing software first, the height channel was
246 selected. A polynomial fit was chosen to be subtracted from each line to obtain straightened scan

247 lines. These images were then further analyzed by Gwyddion SPM data processing software to
248 obtain the size (height, diameter and calculated effective diameter) and number of EVs. The
249 height threshold was selected on gold grains, to eliminate the roughness of the surface. Usually
250 our rough gold substrate (RMS around 3 nm) and the presence of the chemical and the ligand
251 layers bring us to choose a threshold at 8.5 nm.

252
253 The result of this AFM characterization consists in a) counting the EVs number present on each
254 AFM image of $3 \times 3 \mu\text{m}^2$ and for the 10 images collected on each spot), and b) in measuring their
255 size (measured diameter & measured height giving a calculated effective diameter). To reach
256 that, we generate graphs showing the size (measured height, measured diameter and calculated
257 effective diameter) of EVs, with each particles counted represented by a dot.

258 An approach of estimating the effective diameter based on the calculation of the effective
259 volume of the object is adopted as reported in the literature [3]. The “effective diameter” was
260 calculated in two steps. In Gwyddion software, with the grain extraction module, the grains were
261 marked by a height threshold value. Then several properties of the marked grains such as height,
262 diameter were extracted. In the second step, with these values, the volume of the grains was
263 estimated. Then an “effective diameter” equivalent to a sphere of the same volume was derived.

264
265 **[Here Figure 4]**

266
267 Thus, at the end of our characterization, the NBA platform enables to correlate the biodetection
268 signal, and then the phenotyping, to a number and the size of EVs subsets.

269 **REPRESENTATIVE RESULTS:**

270 **Determination of the optimum pH conditions for ligand grafting**

271 The different ligands used to prepare the biochips are tested function of the pH and their
272 availability to interact with the thiolates chemical layer. For that, the ligands are diluted in acetate
273 buffer at different pH and injected on the biochip chemically functionalized with C11C16 layer.
274 The solutions are injected randomly on the surface, and a detergent (octylglucoside at 40mM) is
275 injected after each ligand injection to recover the baseline. This “pre-concentration” test allows
276 to determine the optimal for each ligand grafting. In the example presented in the figure 5, pH6
277 was selected as the better pH for this ligand grafting.

278
279 **[Here Figure 5]**

280 **SPRi CCD images**

281
282 The SPRi CCD images registered on biochip (naked, chemically functionalized or presenting
283 microarrays) once inserted in the SPRi machine, are presented in figure 4. In the case of
284 microarrays presenting biochip, the image is taken after albumin passivation of the surface.
285 Duplicate or triplicate of spots are systematically realized on the chip, and a negative control is
286 automatically also present on the chip. The negative control consists in a irrelevant antibody most
287 of the time.

288
289 In SPRi, when the biochip is used without spotting - for adsorption on naked gold or for grafting

290 directly EVs on chemical functionalized biochip -, ROI are chosen arbitrarily in the sensing area.
291 As an example in figure 6C are represented ROI chosen on a naked gold chip before injection of
292 EVs.

293 **[Here Figure 6]**

294
295 Thanks to this SPRi CCD image, we have then the possibility to ignore certain spots if such
296 mentioned problems appeared during the grafting. The SPRi CCD image allows also to estimate
297 the homogeneity of the grafting inside the spot, the reproducibility of grafting between the
298 different spots of a same ligand, and finally to ensure that EVs biodetection will be proceed on
299 equivalent arrays in terms of surface density.

300
301

302 **SPRi results**

303 When ROI are selected, the baseline is stable, then the sample can be injected. The figure 7 shows
304 different results, obtained on a multiplexed biochip revealing a high signal-to-noise ratio, for
305 certain immunoarrays (the reflectivity signal being xx compared to the response on negative
306 control that is xx). In figure 7B is presented the result in EVs adsorption, obtained after injection
307 of EVs sample on a naked gold chip.

308
309

310 **[Here Figure 7]**

311 **AFM characterization**

312 After SPRi experiments and EVs loading on biochip (either by adsorption, grafting or affinity
313 capture), AFM is engaged, following the methodology to scan firstly big scans ($10 \times 10 \mu\text{m}^2$) then
314 further (around 10 at least) smaller ones (few μm^2). Figure 8 shows example of large and small
315 scale AFM images of EVs on biochips.

316
317

318 **[Here Figure 8]**

319 **Gwyddion analysis**

320 Gwyddion software was used to process the data for each vesicles visualized on every batches of
321 AFM images. Measured height and Diameter of each EVs were determined, from which the
322 effective diameter was obtained.

323 In the software we have first to select "data treatment", then "Grains", then "Label with
324 threshold", then the threshold value has to be adjusted. We determined that 8.5nm was a good
325 one. Then the grains have to be "filtered", and the "number of grains" appears. In "grain
326 distribution" the height volume and diameter of grains have to be selected. Thus, a table
327 presenting 3 columns with Height, Volume and Diameter values for all the grains detected at this
328 threshold, per image, is obtained, in txt format.

329

330 **FIGURE AND TABLE LEGENDS:**

331 **Figure 1** : the NanoBioAnalytical (NBA) Platform combining Surface Plasmon Resonance imaging
332 (SPRi) (A), Atomic Force Microscopy (AFM) (C) and infrared/Raman (nano)spectroscopy, all
333 engaged on the same substrate, a multiplexed gold chip (B).

334

335 **Figure 2:** Gold biochip (left), micropipette spotter (middle) and the biochip after spotting with
336 ligands droplets of 300 nl each (right).

337

338 **Figure 3:** Biochip characterization by AFM. After SPRi experiment, the chip is either fixed and
339 dried or maintained in liquid for AFM characterization. (A) The glass slide machined (with 2
340 perpendicular positioning wedges, indicated with a “w” on the picture) and presenting a mask
341 fitting with the localization of the biochip 16 microarrays. By light exposure and transparency, it
342 enables, once installed for the AFM characterization, to place the AFM tip on the desired spot to
343 characterize. (B) The biochip installed on the “mask” slide and under a drop of buffer, to scan in
344 liquid conditions. (C) SPRi image of the 16 microarrays. (D) One microarray imaged by optical
345 microscopy after immunocapture of biofunctionalized calibration nanoparticles of 920nm in
346 diameter. The white squares indicate the sampling of the different areas scanned by AFM into
347 each spots of interest to make the AFM characterization robust.

348

349 **Figure 4:** Results generated by the AFM characterization of EVs on a biochip. (A) Metrology of
350 EVs on one spot (antiCD41 immunoarray), determined with a threshold of 8.5nm and after
351 injection of EVs sample at 10e8/ml. From the top to the bottom are presented measured particles
352 diameter, effective calculated diameter and height. (B) Histogram generated from the data in (A),
353 showing the distribution of EVs in effective diameter. Results obtained in air (in red: sample fixed
354 and dried) and in liquid (in blue : unfixed).

355

356 **Figure 5:** Pre-concentration tests led in Biacore 3000 SPR apparatus to determine the optimal pH
357 for ligand grafting. The sensorgram present the level of interaction function of time of one ligand
358 injected randomly (in pH) at the same concentration and during 2 min on the surface. OG is the
359 detergent allowing to recover the baseline between each injection.

360

361 **Figure 6:** SPRi CCD image of the biochip. (A & B) Multiplexed biochip, after albumin passivation.
362 In (A) a chip with no default ; in (B) some defaults that can appear on the chip : fusion of spots
363 (i), weak grafting (ii) or dusts or “contaminants” (iii). The ROI, in color in the spots (one color per
364 ligand family), are choosen avoiding those “contaminants”. When spots fusionned, we notify it
365 and the spots are either ignored or named as “mixture of ligands 1 & 2”. (C) Naked gold chip
366 without microarrays, for experiment consisting in adsorption of EVs on gold. The blue arrow
367 indicates the flow direction. This chip does not present spots, and ROI are chosen to register the
368 reflectivity signal from the line 1 (L1, red circles) to the line 4 (L4, purple circles) during the sample
369 injection.

370

371 **Figure 7:** SPRi experiments of EVs injection on biochip. (A) Capture experiment on multiplexed
372 biochip, showing reflectivity signal on different ligands. Here the signal-to-noise ratio for the
373 different ligand is really good (and especially on antiCD41 spots) since the response on the
374 negative control is negligible. (B) Adsorption experiment of EVs on naked biochip. Sensorgram
375 presenting the reflectivity of the chip after the EVs sample injection (4), and after conditioning

376 the chip with 2 flushes of buffer (1 & 2) and OG cleaning (3). On this biochip there is no negative
377 control, but the reflectivity signal (its kinetics, its stability after injection) is high, meaning that
378 those EVs are able to adsorb and stay on gold chip.

379

380 **Figure 8:** AFM characterization of EVs on biochip (here images obtained in contact mode on dried
381 sample). (A) One example of large scanned area to have a representative view of the mm² ROI
382 on chip. This result was obtained after covalent grafting of EVs on chemically modified surface.
383 (B) Another example of large scanned area obtained after capture of EVs on immunoarrays. (C)
384 A closer view of the objects to get high resolution and enabling the metrology (in height &
385 diameter) of EVs. (D) A closer view of the biochip given the image in (A), with a 3D tilted image.
386 (E) A zoom on one large EVs adsorbed on naked gold biochip, on a tilted 3D image. Z scale is 30
387 nm and 20 nm for A, B and C images respectively.

388

389 **DISCUSSION:**

390 The NBA platform, combining biodetection of EVs on multiplexed gold substrate and AFM
391 characterization, enables a deep qualification of nanovesicles present in complex biological
392 fluids. Indeed, thanks to the selectivity of the biochip, crude samples can be injected, and the
393 vesicle contribution to be highlighted.

394

395 Our approach consists then to characterize EVs adsorbed/grafted or captured by affinity, on a
396 rough gold substrate. AFM, that is conventionally used on atomically flat substrate, shows here
397 all its performance on rough gold chip, presenting different sort of interfaces and being
398 micro/nanostructured.

399 Also, the multiplexed biochip presenting several spots to scan (until 16 up to now), we have been
400 developing our NBA approach on fixed and dried sample due to the time needed for a deep &
401 highly resolved AFM investigation of each spot. Different tests realized in the lab showed that
402 this procedure (fixation, drying and imaging in air) does not impact significantly the metrology of
403 EVs.

404

405 There are two main critical steps in our approach: a compromise to select the chip sensitivity for
406 all the different grafted ligand, and the EVs dissociation from the substrate at the end after
407 injection.

408 Indeed, we use a SPRi machine working with one single angle of resonance, meaning that we
409 have to select the better compromise in plasmon response on all the ligands spots ; for some
410 ligands the detection will be really sensitive (close to the angle), for others less sensitive if the
411 fixed angle value is farer than the others.

412 The second critical step is the dissociation of EVs from the substrate, after injection. If the
413 dissociation is too high (because EVs present, for example, only few specific proteins at their
414 surface), we won't be able to scan them afterwards. These situations are really rare, but when it
415 happens, we worked at different flow rate and injection duration, to work around the problem.

416

417 The limitation of our method could rely in the representability of the AFM observations
418 compared to the mm² area of EVs interaction on the biochip. For that we have absolutely to scan
419 different areas on the spot, from big to small ones and at different places inside the spot. We

420 even try to scan in the ROI area, for the AFM characterization to be as much as possible correlated
421 to SPRi response.

422
423 This coupled & label-free approach, assisted by a rigorous methodology in the preparation of the
424 biochip and in the AFM acquisition mode, constitutes a method of choice to characterize EVs in
425 sample even complex and crude. Thus, no preanalytical steps on the sample, no labelling or
426 exalting procedure are needed in our method, while EVs subsets are deeply characterized. These
427 different elements place our NBA platform as a very relevant method for deep and resolved
428 analysis of EVs directly in crude sample.

429
430 Our recent developments consists in improving the sensitivity in biodetection and the
431 discrimination between EVs subsets coexisting in a sample, that potentially co-interact on the
432 same arrays. To increase the sensitivity, we are switching currently from the SPRiPlex instrument
433 to a XelPlex one, that enables to select several angles for EVs detection on the different spots.
434 To improve the discrimination of EVs subsets, we are facing different challenges : a) getting the
435 infrared & raman signature of each EVs subsets on biochip, b) increasing the number of spots
436 realized on the biochip (from 16 to 100) and c) increasing the throughput of analysis thanks to
437 high-speed AFM. Moreover, HS AFM will then allow also to characterize EVs subsets, rapidly, and
438 in liquid condition.

439
440 **ACKNOWLEDGMENTS:**
441 The work was supported by the region Bourgogne Franche Comté and the EUR EIPHI graduate
442 school (NOVICE project, 2021-2024). Part of this work was done in RENATECH clean room
443 facilities.

444
445 **DISCLOSURES:**
446 The authors have nothing to disclose.

447
448 **REFERENCES:**

449
450 [1] W Boireau, C Elie-Caille, Extracellular vesicles: Definition, isolation and characterization
451 *Medecine Sciences: M/S*, 2021, 37 (12), 1092-1100

452
453 [2] Brisson AR, Tan S, Linares R, et al. Extracellular vesicles from activated platelets: a
454 semiquantitative cryo-electron microscopy and immuno-gold labeling study. *Platelets* (2017),
455 28(3) : 263-71.

456
457 [3] Yuana Y, Oosterkamp TH, Bahatyrova S, et al. Atomic force microscopy: A novel approach to
458 the detection of nanosized blood microparticles. *Journal of Thrombosis and Haemostasis*. (2010),
459 8(2):315-323. doi:10.1111/j.1538-7836.2009.03654.x

460
461 [4] Sebaihi N, de Boeck B, Yuana Y, Nieuwland R, Pétry J. Dimensional characterization of
462 extracellular vesicles using atomic force microscopy. *Measurement Science and Technology*.
463 (2017);28(3):034006. doi:10.1088/1361-6501/28/3/034006

464
465 [5] Beekman P, Enciso-Martinez A, Rho HS, et al. Immuno-capture of extracellular vesicles for
466 individual multi-modal characterization using AFM, SEM and Raman spectroscopy. *Lab on a Chip.*
467 (2019);19(15):2526-2536. doi:10.1039/c9lc00081j
468
469 [6] Malenica M, Vukomanović M, Kurtjak M, et al. Perspectives of Microscopy Methods for
470 Morphology Characterisation of Extracellular Vesicles from Human Biofluids. *Biomedicines*
471 (2021), 9(6) : 603.
472
473 [7] Verweij, FJ; Balaj, L, ... Van Niel, G. The power of imaging to understand extracellular vesicle
474 biology in vivo, (2021) *NATURE METHODS* 18 (9), pp.1013-1026
475
476 [8] Théry C, ...Boireau W, ... ELIE-CAILLE C., ... and Zuba-Surma EK. Minimal information for studies
477 of extracellular vesicles 2018 (MISEV2018): a position statement of the International Society for
478 Extracellular Vesicles and update of the MISEV2014 guidelines, *Journal of Extracellular Vesicles*
479 (2018) VOL. 8, 1535750
480
481 [9] Obeid S., Sung, P-S., Le Roy B., Chou M-L., Shieh S-L., ELIE-CAILLE C., Burnouf T., Boireau W.
482 NanoBioAnalytical characterization of extracellular vesicles in 75-nm nanofiltered human plasma
483 for transfusion: a tool to improve transfusion safety. *Nanomedicine: Nanotechnology, Biology,*
484 *and Medicine* (2019) pii: S1549-9634(19)30061-9.
485
486 [10] Obeid S, Ceroi A, Mourey G, Saas P., Elie-Caille C., Boireau W. Development of a
487 NanoBioAnalytical platform for «on-chip» qualification and quantification of platelet-derived
488 microparticles. *Biosens Bioelectron.* (2017), 93:250-259
489
490 [11] Ridolfi, A; Brucale, M; (...); Valle, F, AFM-Based High-Throughput Nanomechanical Screening
491 of Single Extracellular Vesicles (2020), *Analytical Chemistry*, 92 (15), pp.10274-10282.
492
493 [12] Vorselen, D; van Dommelen, SM; (...); Roos, WH, The fluid membrane determines mechanics
494 of erythrocyte extracellular vesicles and is softened in hereditary spherocytosis (2018), *Nature*
495 *Communications*, 9, 4960, DOI 10.1038/s41467-018-07445-x
496
497 [13] Hardij J, Cecchet F, Berquand A, et al. Characterisation of tissue factor bearing extracellular
498 vesicles with AFM : comparison of air-tapping-mode AFM and liquid Peak Force AFM. *J Extracell*
499 *Vesicles* (2013) ; 2 : 21045.
500
501 [14] Jorgensen M, Bæk R, Pedersen S, et al. Extracellular Vesicle (EV) Array: microarray capturing
502 of exosomes and other extracellular vesicles for multiplexed phenotyping. *J Extracell Vesicles*
503 (2013) ; 2 : 20920
504
505 [15] Remy-Martin F, el Osta M, Lucchi G, et al. Surface plasmon resonance imaging in arrays
506 coupled with mass spectrometry (SUPRA-MS): Proof of concept of on-chip characterization of a
507 potential breast cancer marker in human plasma. *Analytical and Bioanalytical Chemistry*

508 (2012);404(2):423-432. doi:10.1007/s00216-012-6130-4
509

Figure 1

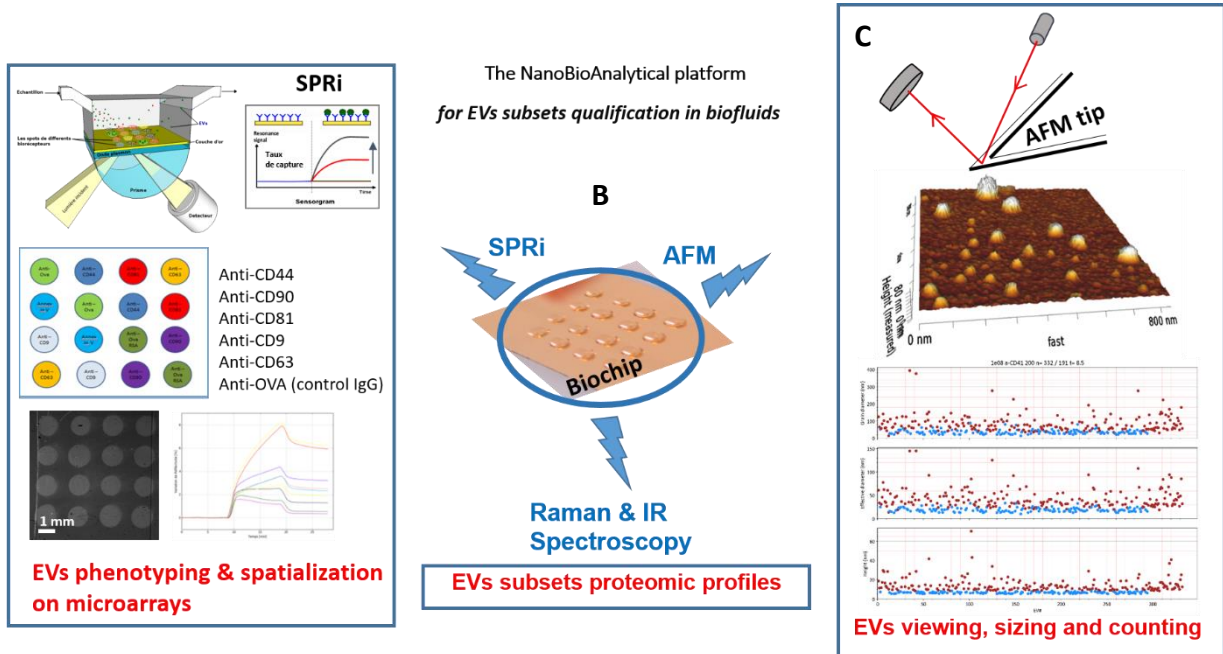


Figure 1 : the NanoBioAnalytical (NBA) platform combining Surface Plasmon Resonance imaging (SPRi) (A), Atomic Force Microscopy (AFM) (C) and infrared/Raman (nano)spectroscopy, all engaged on the same substrate, a multiplexed gold chip (B).

Figure 2



Figure 2: Gold biochip (left), micropipette spotter (middle) and the biochip after spotting with ligands droplets of 300 nl each (right).

Figure 3

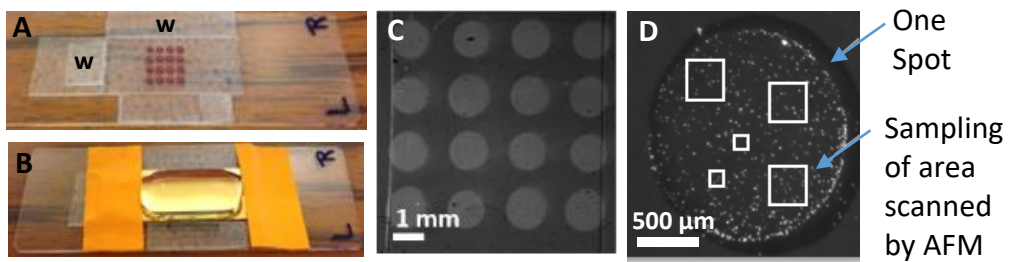


Figure 3: Biochip characterization by AFM. After SPRi experiment, the chip is either fixed and dried or maintained in liquid for AFM characterization. (A) The glass slide machined (with 2 perpendicular positioning wedges, indicated with a “w” on the picture) and presenting a mask fitting with the localization of the biochip 16 microarrays. By light exposure and transparency, it enables, once installed for the AFM characterization, to place the AFM tip on the desired spot to characterize. (B) The biochip installed on the “mask” slide and under a drop of buffer, to scan in liquid conditions. (C) SPRi image of the 16 microarrays. (D) One microarray imaged by optical microscopy after immunocapture of biofunctionalized calibration nanoparticles of 920nm in diameter. The white squares indicate the sampling of the different areas scanned by AFM into each spots of interest to make the AFM characterization robust.

Figure 4

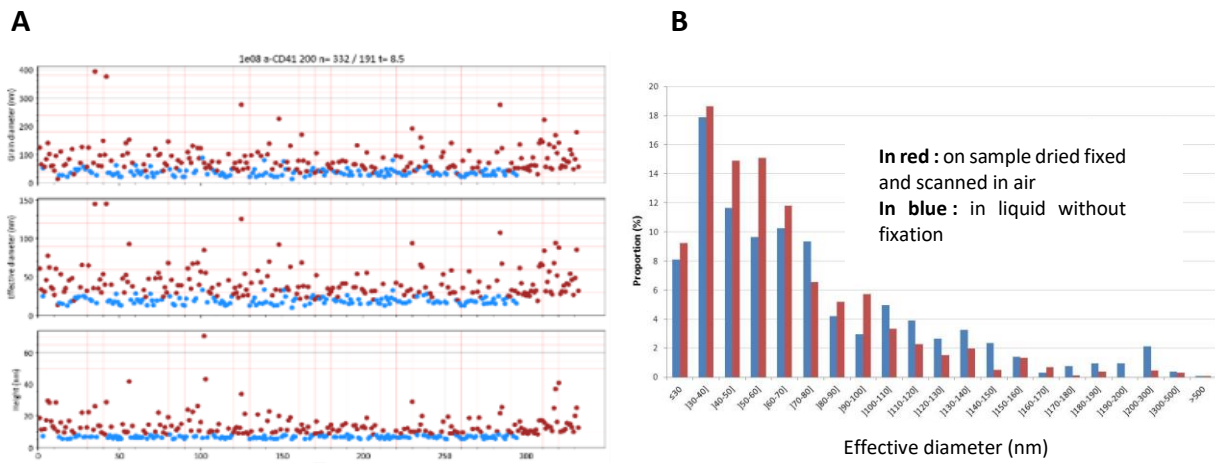


Figure 4: Results generated by the AFM characterization of EVs on a biochip. (A) Metrology of EVs on one spot (antiCD41 immunoarray), determined with a threshold of 8.5nm and after injection of EVs sample at 10e8/ml. From the top to the bottom are presented measured particles diameter, effective calculated diameter and height. (B) Histogram generated from the data in (A), showing the distribution of EVs in effective diameter. Results obtained in air (in red: sample fixed and dried) and in liquid (in blue : unfixed).

Figure 5

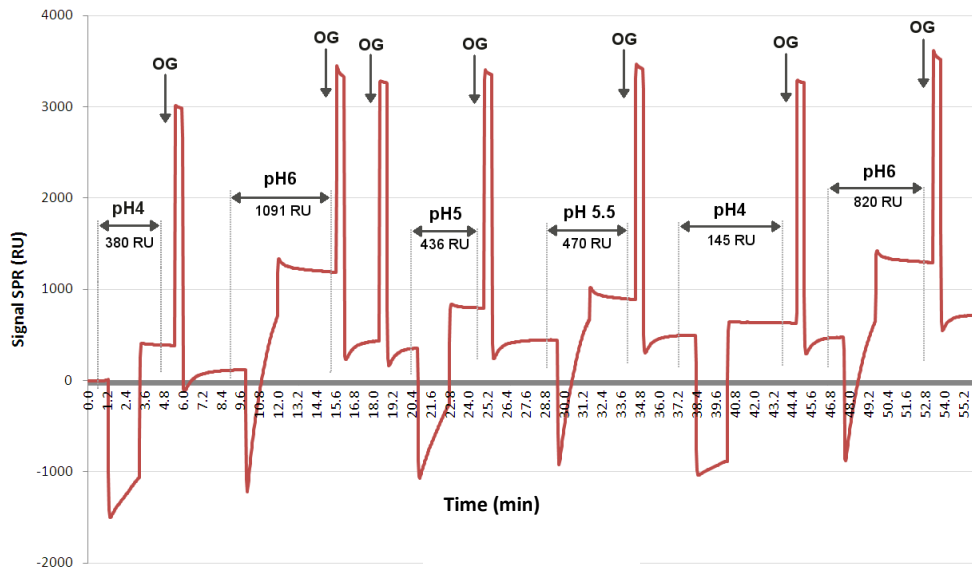


Figure 5 : Pre-concentration tests led in Biacore 3000 SPR apparatus to determine the optimal pH for ligand grafting. The sensorgram present the level of interaction function of time of one ligand injected randomly (in pH) at the same concentration and during 2 min on the surface. OG is the detergent allowing to recover the baseline between each injection.

Figure 6

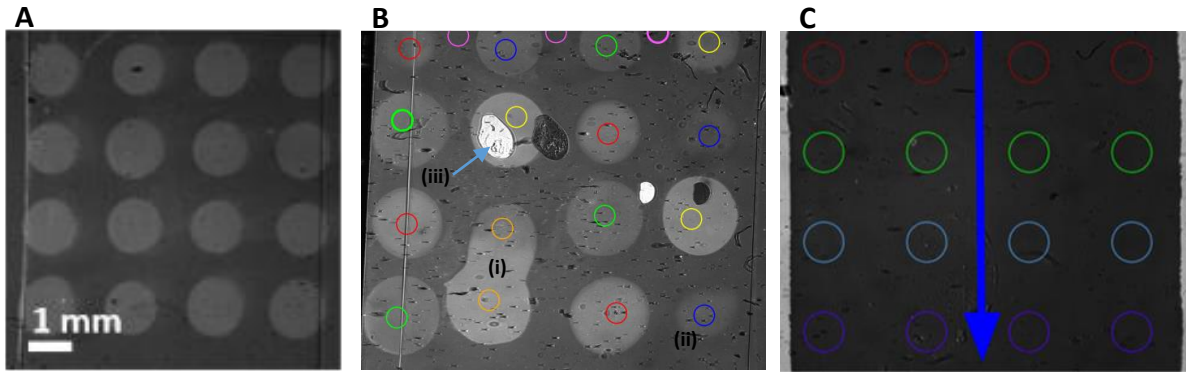


Figure 6 : SPRi CCD image of the biochip. (A & B) Multiplexed biochip, after albumin passivation. In (A) a chip with no default ; in (B) some defaults that can appear on the chip : fusion of spots (i), weak grafting (ii) or dusts or “contaminants” (iii). The ROI, in color in the spots (one color per ligand family), are chosen avoiding those “contaminants”. When spots fusionned, we notify it and the spots are either ignored or named as “mixture of ligands 1 & 2”. (C) Naked gold chip without microarrays, for experiment consisting in adsorption of EVs on gold. The blue arrow indicates the flow direction. This chip does not present spots, and ROI are chosen to register the reflectivity signal from the line 1 (L1, red circles) to the line 4 (L4, purple circles) during the sample injection.

Figure 7

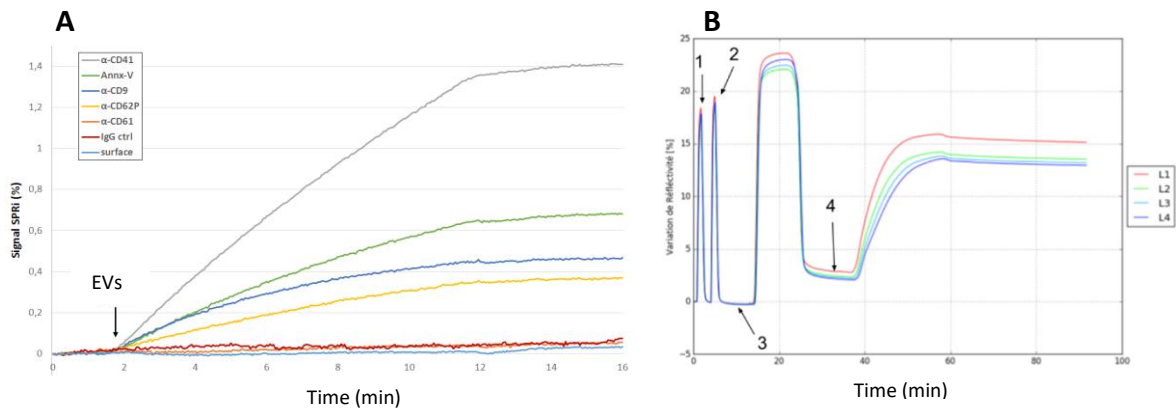


Figure 7: SPRi experiments of EVs injection on biochip. (A) Capture experiment on multiplexed biochip, showing reflectivity signal on different ligands. Here the signal-to-noise ratio for the different ligand is really good (and especially on antiCD41 spots) since the response on the negative control is negligible. (B) Adsorption experiment of EVs on naked biochip. Sensorgram presenting the reflectivity of the chip after the EVs sample injection (4), and after conditioning the chip with 2 flushes of buffer (1 & 2) and OG cleaning (3). On this biochip there is no negative control, but the reflectivity signal (its kinetics, its stability after injection) is high, meaning that those EVs are able to adsorb and stay on gold chip.

Figure 8

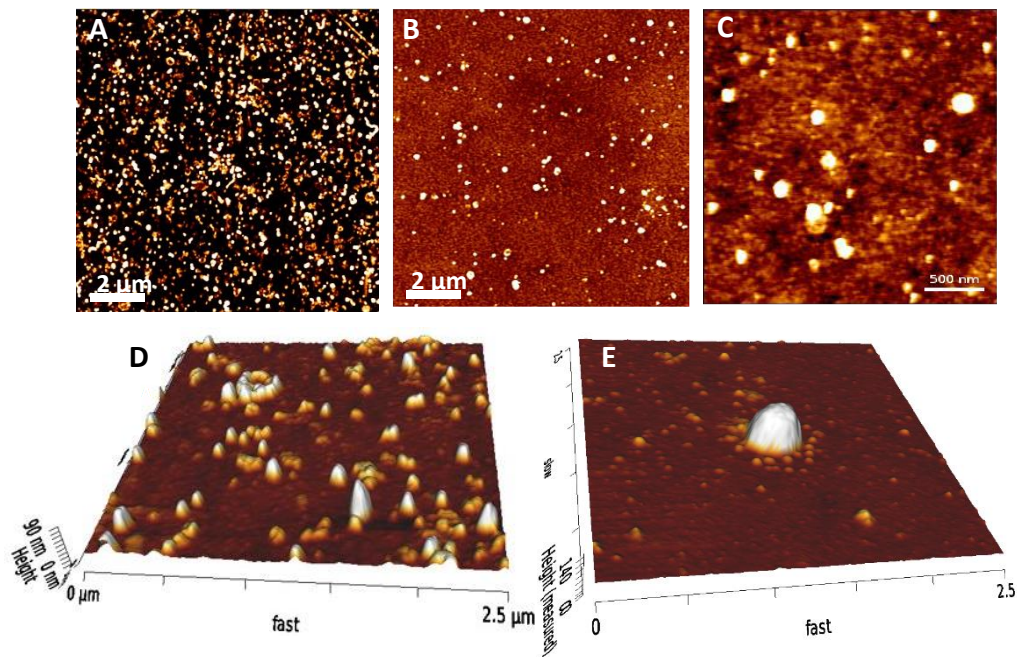


Figure 8: AFM characterization of EVs on biochip (here images obtained in contact mode on dried sample). (A) One example of large scanned area to have a representative view of the mm² ROI on chip. This result was obtained after covalent grafting of EVs on chemically modified surface. (B) Another example of large scanned area obtained after capture of EVs on immunoarrays. (C) A closer view of the objects to get high resolution and enabling the metrology (in height & diameter) of EVs. (D) A closer view of the biochip given the image in (A), with a 3D tilted image. (E) A zoom on one large EVs adsorbed on naked gold biochip, on a tilted 3D image. Z scale is 30 nm and 20 nm for A, B and C images respectively.